**© 2020 IEEE. Personal use of this material is permitted. Permission from IEEE must be obtained for all other uses, in any current or future media, including reprinting/republishing this material for advertising or promotional purposes, creating new collective works, for resale or redistribution to servers or lists, or reuse of any copyrighted component of this work in other works.**

# Synthesizing Shaped Power Patterns for Linear and Planar Antenna Arrays Including Mutual Coupling by Refined Joint Rotation/Phase Optimization

Yanhui Liu, *Senior Member, IEEE*, Ming Li, Randy L. Haupt, *Fellow, IEEE*, and Y. Jay Guo, *Fellow, IEEE*

***Abstract*—In this paper, a novel strategy based on refined joint element rotation/phase optimization is presented to obtain vectorial shaped power patterns for antenna arrays with arbitrary element structures including mutual coupling. The active element pattern (AEP) is used for each antenna element, and then the rotation of an element is approximately described by mathematically rotating its AEP under the assumption that the mutual coupling variation does not change the AEP considerably. Optimal element rotations and phases for an array can be found by solving a vectorial shaped pattern synthesis problem such that the obtained array pattern has the desired co-polarization mainlobe shape while maintaining constrained sidelobe and cross-polarization levels. However, due to the variation of mutual coupling, this synthesized pattern may deviate from the real array pattern. To reduce the pattern discrepancy, successive refined joint element rotation/phase optimizations are adopted. As the number of refining steps increases, the allowable element rotation range is set to be smaller and smaller so that the synthesized array pattern can get closer and closer to the real one. Such a shaped power pattern synthesis technique does not need nonuniform amplitude weighting, thus saving many unequal power dividers. Three examples for synthesizing rotated linear and planar arrays with different antenna structures and different pattern shape requirements are provided to validate the effectiveness and advantages of the proposed method.**

***Index Terms*—Shaped power pattern synthesis, rotated antenna array, joint rotation/phase optimization, active element pattern (AEP), cross-polarization level (XPL)**

## I. Introduction

ANTENNA arrays with desired power pattern shapes are required in many applications such as satellite communications, sensing and imaging systems. In the past decades, many sophisticated methods have been developed to synthesize various shaped pattern antenna arrays. They include, for example, the analytical techniques [1], [2], alternating projection methods [3], [4], iterative fast Fourier transform (FFT) and its variants [5]-[7], convex optimization techniques [8]-[10], semi-definite relaxation methods [11], [12], and stochastic optimization algorithms [13]-[16]. Since synthesizing shaped patterns is a complicated process, the majority of synthesis methods choose to optimize both excitation amplitudes and phases in order to obtain good control on both the mainlobe shape and sidelobe level. Consequently, the obtained array usually requires a relatively complicated feeding network to implement simultaneous amplitude and phase weighting, and multiple unequal power dividers must be designed with much attention.

To avoid the usage of unequal power dividers, a few methods have been presented to generate shaped beam patterns by performing phase-only optimization such as in [17]-[20]. Owing to the limited degrees of freedom, however, the obtained overall performance in terms of mainlobe shape accuracy, transition width and sidelobe level is usually considerably worse than that obtained with full control of both the excitation amplitudes and phases. In [21], element positions in addition to the phases are optimized to improve the performance of the shaped pattern synthesis.

It is well understood that rotating an antenna element changes the power distributions of both the co-polarized (CoP) and cross-polarized (XP) components of this element for a given observation plane. Hence, element rotation can be considered as a way of providing additional degrees of freedom for array pattern synthesis. In [22] and [23], arrays with rotated ideal dipoles are synthesized for obtaining low sidelobe level (SLL) focused patterns. In [25]-[27], authors used sequential element rotation to generate circular polarization (CP) radiation from rotated, phased, linearly polarized elements. However, these techniques so far consider only focused beam patterns using a precalculated excitation phases, and they cannot be directly used to deal with more complicated shaped pattern problems. More recently, in [27], we presented one optimization strategy in which the element rotations along with phases are jointly optimized using a dynamic differential evolution (DDE) to produce a desired CoP shaped pattern under the constraints on the SLL and cross-polarization level (XPL). This method avoids the use of multiple unequal power dividers and significantly simplifies the feeding network. However, the method in [27] deals with only ideal rotated dipole antenna arrays where analytical expressions are adopted for the rotated element and array patterns. Hence, practical antenna arrays with different structures and mutual coupling effects cannot be handled by this method. Besides, since the formulation and synthesis examples shown in [27] are only for linear rotated dipole array cases, the effectiveness of the idea of joint

Manuscript received xxx. This work was supported in part by the Natural Science Foundation of China (NSFC) under Grant No. 61871338, in part by the Science and Technology Research Project of Fujian Province under Grant No 2017I0017, and in part by the University of Technology Sydney.

Y. Liu is with the Global Big Data Technologies Centre, University of Technology Sydney (UTS), NSW 2007, Australia, and also with the School of Electronic Science and Engineering, University of Electronic Science and Technology of China, Chengdu 611731, China. (email: yhliu@uestc.edu.cn).

M. Li and Y. Jay Guo are with the Global Big Data Technologies Centre, University of Technology Sydney (UTS), NSW 2007, Australia. (email: ming.li-1@student.uts.edu.au; jay.guo@uts.edu.au)

R. L. Haupt is with Electrical Engineering and Computer Science, Colorado School of Mines, Golden, CO 80401, USA. (email: rhaupt@mines.edu)

rotation-phase optimization for more general arrays such as planar arrays including mutual coupling is worthy of further study.

In this paper, we further extend the idea of joint rotation-phase optimization to synthesize vectorial shaped power patterns for linear and planar antenna arrays with arbitrary element structures. The active element pattern (AEP) is used for each antenna element in an array environment to include mutual coupling [28], [29], and rotating an element is approximated as mathematically rotating the AEP of this element by assuming that the mutual coupling from nearby elements does not change the element pattern very much. The accuracy of such an assumption would depend on the rotation angle range for a given element structure and position distribution. When the rotation angle gets smaller, the approximation accuracy will be much higher. Hence, a successive refined joint rotation-phase optimization strategy is proposed. That is, once the optimized rotations and phases are obtained, one can employ full-wave simulation to obtain the real AEPs for the new array configuration, and thus the rotations and phases can be further adjusted based on the updated rotated array pattern approximation by using the new AEPs. To reduce the discrepancy between the synthesized and real array patterns, the allowable rotation range is set to be smaller and smaller as the number of refining steps increases. Several examples for synthesizing vectorial shaped patterns for different linear and planar antenna arrays are conducted. The synthesis results show that only few refining steps are required for the proposed method to achieve satisfactory shaped array patterns.

## II. Formulation and Algorithm

This section presents the antenna array model used in the evaluation of fitness function as well as the refined element rotation/phase synthesis procedure based on particle swarm optimization (PSO) optimization.

### A. Vectorial pattern of a rotated antenna array

Consider an antenna array with $N$ rotated elements located in the $xy$-plane. As an illustration, Fig. 1(a) shows a 3×3 element-rotated planar patch array. This array can be regarded as the one obtained by separately rotating each element of a conventional array without element rotation shown in Fig.1(b) in the $xy$-plane about the $z'$-axis of the local coordinate system. Assume that the rotation angles are $\xi_n$ for $n = 1, 2, \cdots, N$. The vectorial array pattern can be given by

$$\vec{F}^{\text{Rot}}(\theta,\phi) = \sum_{n=1}^{N} \vec{E}_n(\theta,\phi;\xi_n) e^{j\{\beta \vec{r}_n \cdot \vec{u}(\theta,\phi)+\alpha_n\}} \quad (1)$$

where $j = \sqrt{-1}$, $\beta = 2\pi/\lambda$ is the wavenumber in free space, $\vec{u}(\theta,\phi) = \sin\theta\cos\phi\vec{e}_x + \sin\theta\sin\phi\vec{e}_y + \cos\theta\vec{e}_z$ is the propagation direction vector. $\vec{r}_n$ and $\alpha_n$ are the location and excitation phase of the $n$th element, respectively. In the above, $\vec{E}_n(\theta,\phi;\xi_n) = E_{n,\theta}(\theta,\phi;\xi_n)\vec{e}_\theta + E_{n,\phi}(\theta,\phi;\xi_n)\vec{e}_\phi$ is the phase-adjusted AEP for the $n$th antenna with the rotation angle of $\xi_n$ (the coordinate origin is located at each element [28], and $\xi_n > 0$ denotes an anticlockwise rotation). The AEP is defined as the pattern of an array when only one element is excited and all the others are connected to matching loads. By using the concept of AEP, the array pattern expression in (1) can include the mutual coupling even for a complicated array geometry with rotated antenna elements.

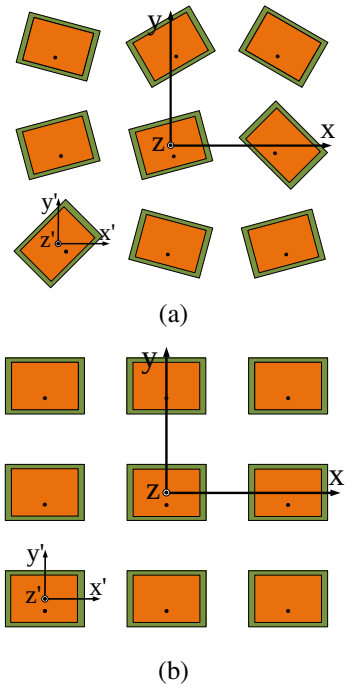


Fig. 1. Configuration of 3×3 planar arrays with (a) rotated elements, and (b) without element rotation.

In the array environment, the AEPs vary among different elements. For an element-rotated array, the AEP of an antenna element depends not only on its own rotation angle but also on the rotation angles of other elements especially in nearby region. In general, the AEPs can be obtained by using full-wave simulation or measurement. However, in the concerned problem of synthesizing a shaped pattern by using joint optimization of element rotations and phases, the element rotations and phases are unknown variables. Hence, we do not actually know their values. To deal with this issue, we can make an assumption that when an element is rotated, the mutual coupling variation between this element and nearby elements does not change the AEP very much. Thus, the pattern of a rotated element can be approximately obtained by mathematically rotating the original AEP of this element from its '0' rotation state. That is, the phase-adjusted AEP for the $n$th rotated element can be approximated as

$$\vec{E}_n(\theta,\phi;\xi_n) \approx E_{n,\theta}(\theta,\phi-\xi_n;0)\vec{e}_\theta + E_{n,\phi}(\theta,\phi-\xi_n;0)\vec{e}_\phi \quad (2)$$

where $E_{n,\theta}(\theta,\phi;0)$ and $E_{n,\phi}(\theta,\phi;0)$ are the $\vec{e}_\theta$- and $\vec{e}_\phi$-polarization components of the AEP for the $n$th element with '0' rotation state.

By substituting (2) into (1), we obtain that

$$F_\theta^{\text{Rot}}(\theta,\phi) \approx \sum_{n=1}^{N} E_{n,\theta}(\theta,\phi-\xi_n;0) e^{j\{\beta \vec{r}_n \cdot \vec{u}(\theta,\phi)+\alpha_n\}} \quad (3)$$

$$F_{\phi}^{\mathrm{Rot}}(\theta,\phi) \approx \sum_{n=1}^{N} E_{n,\phi}(\theta,\phi-\xi_n;0)e^{j\{\beta\vec{r}_n\cdot\vec{u}(\theta,\phi)+\alpha_n\}}. \quad (4)$$

In the above, the approximation accuracy depends on the rotation angles of $\xi_n$ for $n = 1, 2, \cdots, N$, provided that the element spacings and radiating structures are determined. Usually, increasing the rotation angle reduces the approximation accuracy. Consequently, a fitness function that optimizes the element rotations and phases based on the approximations in (3) and (4) causes the real array pattern to deviate from the synthesized pattern due to changes in mutual coupling. Such pattern discrepancy depends heavily on the allowable range of the rotation angle $\xi_n$. Naturally, a refining step can be done to reduce the discrepancy. For instance, once the optimized element rotations and phases using the approximated expressions are obtained, one can employ full-wave simulation to obtain all the real AEPs for the new configurations. Then the element rotations can be further adjusted within a smaller range to reduce the discrepancy between the synthesized and real array patterns.

Clearly, such a refined joint rotation/phase optimization can be performed multiple times until the discrepancy between the synthesized and real array patterns becomes negligible or less than a prescribed tolerance. Assume that the rotation angle for the $n$th element is $\xi_n^{(0)}$ at the initial rotation step and $\xi_n^{(k)}$ at the $k$th refining step ($k = 1, 2, \cdots, K$), and the element phase for the $n$th element is $\alpha_n^{(0)}$ at the initial rotation step and $\alpha_n^{(k)}$ at the $k$th refining step. Then, the approximated array pattern at $k$th refining step is given by

$$F_{\nu}^{(k)}(\theta,\phi) \approx \sum_{n=1}^{N} E_{n,\nu}(\theta,\phi-\xi_n^{(k)};\sum_{l=0}^{k-1}\xi_n^{(l)})e^{j\{\beta\vec{r}_n\cdot\vec{u}(\theta,\phi)+\alpha_n^{(k)}\}} \quad (5)$$

where $\nu = [\theta, \phi]$, and $F_{\nu}^{(k)}$ denotes $F_{\theta}^{(k)}$ or $F_{\phi}^{(k)}$. In the successive refining optimization process, the allowed range of $\xi_n^{(k)}$ can be set to be smaller and smaller as $k$ increases. When the allowed range of $\xi_n^{(k)}$ becomes small enough, the synthesized array pattern will agree well with the real one including mutual coupling variation.

### *B. Vectorial shaped pattern synthesis using joint rotation/phase optimization*

In the problem of synthesizing a vectorial shaped pattern using joint element rotation/phase optimization, the optimal rotations and phases can be found such that the synthesized pattern has the CoP component approaching to a desired mainlobe shape as close as possible, while both of the maximum SLL and XPL are constrained as well. However, one problem is that a user-defined desired polarization denoted by $\vec{p}_d$ is usually a fixed direction depending on the application, but the realizable CoP direction radiated by an actual antenna array is always perpendicular to the propagation direction $\vec{u}(\theta, \phi)$ and it varies with the changing of $\vec{u}(\theta, \phi)$. Thus, if we view the realizable CoP in wide-angle space, it is usually different from the fixed user-defined desired polarization. To facilitate the formulation of the vectorial shaped pattern synthesis problem, we adopt a definition of the realizable CoP which was given in

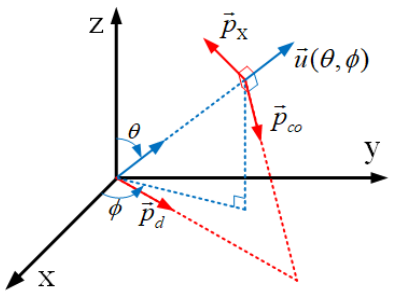


Fig. 2. Illustration of the definitions of CoP and XP directions.

[12]. The realizable CoP is defined as the projection of $\vec{p}_d$ onto the wavefront plane that is perpendicular to the propagation direction $\vec{u}(\theta, \phi)$ [12]. As can be seen in Fig. 2, the CoP is given by

$$\vec{p}_{co} = \frac{\vec{p}_d - [\vec{p}_d \cdot \vec{u}(\theta,\phi)]\vec{u}(\theta,\phi)}{|\vec{p}_d - [\vec{p}_d \cdot \vec{u}(\theta,\phi)]\vec{u}(\theta,\phi)|}. \quad (6)$$

Then the realizable XP direction $\vec{p}_X$ should be perpendicular to both $\vec{p}_{co}$ and $\vec{u}(\theta, \phi)$. It is given by

$$\vec{p}_X = \vec{p}_{co} \times \vec{u}(\theta,\phi). \quad (7)$$

Note that the CoP and XP defined in the above can be regarded as an extension of Ludwig's polarization definition II to a more general case of an arbitrarily desired $\vec{p}_d$ [30]. When $\vec{p}_d = \vec{e}_y$, the above polarization definition reduces to the form of Ludwig's definition II [30].

With the help of the above two definitions, we can obtain the approximated CoP and XP patterns if the elements of a rotated antenna array are further rotated with angles of $\xi_n^{(k)}$ ($n = 1, \cdots, N$) at the $k$th step. The approximated CoP pattern is given by

$$F_{co}^{(k)}(\theta,\phi) \approx \sum_{n=1}^{N} E_{n,co}(\theta,\phi-\xi_n^{(k)};\sum_{l=0}^{k-1}\xi_n^{(l)})e^{j\{\beta\vec{r}_n\cdot\vec{u}(\theta,\phi)+\alpha_n\}} \quad (8)$$

where

$$\begin{aligned} E_{n,co}(\theta,\phi;\textstyle\sum_{l=0}^{k-1}\xi_n^{(l)}) = {} & E_{n,\theta}(\theta,\phi;\textstyle\sum_{l=0}^{k-1}\xi_n^{(l)})\vec{e}_\theta\cdot\vec{p}_{co} \\ & + E_{n,\phi}(\theta,\phi;\textstyle\sum_{l=0}^{k-1}\xi_n^{(l)})\vec{e}_\phi\cdot\vec{p}_{co}. \end{aligned} \quad (9)$$

In the above, $E_{n,\theta}(\theta, \phi; \sum_{l=0}^{k-1} \xi_n^{(l)})$ and $E_{n,\phi}(\theta, \phi; \sum_{l=0}^{k-1} \xi_n^{(l)})$ are obtained using full-wave simulation of the antenna array after the $(k-1)$th refining step. Similarly, the approximated XP pattern $F_{co}^{(k)}(\theta, \phi)$ can be obtained by replacing $\vec{p}_{co}$ with $\vec{p}_X$ in (8) and (9).

In order to achieve the desired shaped power pattern with constrained SLL and XPL for an rotated antenna array, the rotation angles $\xi_n^{(k)}$ and excitation phases $\alpha_n^{(k)}$ at each step should be optimized with an appropriate fitness function. Here the fitness function presented in [27] is extended to deal with the current refined joint rotation/phase optimization problem. Suppose that the desired CoP mainlobe is denoted by $P_t(\theta, \phi)$ and the desired SLL and XPL are denoted by $\Gamma_{SLL}$ and $\Gamma_{XPL}$,

respectively. Then the fitness function at the $k$th step is chosen as

$$f = \frac{W_1}{B}\sum_{b=1}^{B}\{|F_{co}^{(k)}(\theta_b,\phi_b)|^2 - P_t(\theta_b,\phi_b)\}^2 + \frac{W_2}{C}\sum_{c=1}^{C}\frac{1}{2}(X_c+|X_c|)^2 + \frac{W_3}{D}\sum_{d=1}^{D}\frac{1}{2}(Y_d+|Y_d|)^2 \tag{10}$$

where

$$\begin{cases} X_c = |F_{co}^{(k)}(\theta_c,\phi_c)|^2 - \Gamma_{SLL};\ \theta_c,\phi_c \in \text{SLL region} \\ Y_d = |F_{X}^{(k)}(\theta_d,\phi_d)|^2 - \Gamma_{XPL};\ \theta_d,\phi_d \in \text{XPL region.} \end{cases} \tag{11}$$

In the above, $(\theta_b,\phi_b)$ for $b = 1,2,\cdots,B$ are the sampling angles in the shaped mainlobe region of the CoP pattern, $(\theta_c,\phi_c)$ for $c = 1,2,\cdots,C$ are the sampling angles in the sidelobe region, and $(\theta_d,\phi_d)$ for $d = 1,2,...,D$ are the sampling angles in the region of interest where the XPL needs to be controlled. $W_1$, $W_2$, and $W_3$ are weighting factors. In general, using a larger $W_1$ will lead to better approximation of the desired mainlobe shape, but large ratios of $W_1/W_2$ and $W_1/W_3$ may increase the SLL and XPL. Hence, these parameters should be chosen appropriately such that a good overall pattern performance can be achieved.

Minimization of the fitness function in (10) by optimizing rotation angles and excitation phases is a highly non-linear problem. In general, some stochastic optimization algorithms capable of finding the globally optimum solution would be applicable. In this work, a particle swarm optimization (PSO) algorithm is adopted to deal with this optimization problem [31], since it is relatively computationally inexpensive in terms of both memory requirements and speed [32]-[35]. In the PSO based optimization, $N_p$ particles are randomly generated in the beginning and each particle represents one solution of $\{(\xi_n^{(k)},\alpha_n^{(k)});|n=1,2,...,N\}$ . Then guided by the fitness function (10), these particles will iteratively update their velocities and positions to search for better solution of the rotation angles and phases. At last, if the fitness function remains unchanged for multiple iterations or the allowed maximum iteration number $M$ is reached, the optimization procedure will be terminated.

### C. The refined joint rotation/phase optimization strategy

The overall process of the proposed refined joint rotation/phase optimization method are listed in Algorithm 1. At the $k$th step, the rotation range is set as $\xi_n^{(k)} \in s^k[1+\delta(k)][-\pi/2,\pi/2]$ where the parameter $s$ ($0<s<1$) is a scale factor, and $\delta(k)$ is equal to 1 for $k=0$ and 0 for others. In general, selecting a larger $s$ (e.g., close to 1) requires more refining steps to reduce the discrepancy between the synthesized and real array patterns including mutual coupling, which increases the total time cost. On the other hand, selecting a smaller $s$ leads to faster convergence of the proposed procedure but may affect the obtained performance of the array pattern. The effect of using different values of $s$ on the performance of the proposed method will be provided in numerical result part. Note that the time cost of this procedure mainly comes from the full-wave simulation of the antenna array for obtaining the AEP of each element in each step. In the initial step, the AEP can be approximately obtained by using analytical solution or simulation with periodic boundaries, which can reduce the time cost without affecting the final synthesis accuracy.

**Algorithm 1** The proposed refined joint rotation/phase optimization algorithm for vectorial shaped pattern synthesis

1: Set the initial antenna array configurations including element structure, element count and array geometry, and set the desired mainlobe shape $P_t(\theta_b,\phi_b)$, the desired maximum SLL $\Gamma_{SLL}$ and XPL $\Gamma_{XPL}$;
2: Set the parameters for PSO algorithm such as the population size $N_p$, the weighting factors $W_1$, $W_2$ and $W_3$;
3: Find the active element pattern (AEP) for each element by using full-wave simulation, or find approximated element patterns by using either analytical solution or simulation with periodical boundaries;
4: Set $k=0$, and initialize $s=1/3$;
5: Find the optimized element rotation angles $\xi_n^{(k)} \in s^k[1+\delta(k)][-\pi/2,\pi/2]$ and phases $\alpha_n^{(k)} \in [0,2\pi]$ for $n=1,2,\cdots,N$ by minimizing the fitness function (10) using PSO algorithm in order to maximally match the synthesized shaped array pattern and the desired one.
6: Update the element rotation angles $\xi_n^{(k)} = \xi_n^{(k)} + \xi_n^{(k-1)}$ for $n=1,2,\cdots,N$.
7: Use full-wave simulation to obtain the real array pattern with the obtained element rotations $\xi_n^{(k)}$ and phases $\alpha_n^{(k)}$, and find all the AEPs at current states of rotations from this simulation;
8: Check if the discrepancy between the synthesized and real array patterns meet the prescribed tolerance in terms of some characteristics such as the maximum SLL or mainlobe shape deviation. If yes, exit the whole procedure; otherwise, set $k=k+1$ and repeat Step 5 to 8.

## III. Numerical Results

### A. Cosecant-squared pattern synthesis for a rotated dipole array including mutual coupling

In the first example, we synthesize a cosecant-squared pattern that was obtained in [21] by using a linear array with 29 nonuniform positions and phases, as shown in Fig. 3(a). This pattern was also synthesized in [27] by optimizing the element rotations and phases with the help of analytical expression of an ideally rotated dipole array without considering the mutual coupling effect. Now, we apply the proposed refined joint rotation/phase optimization method to synthesize this pattern. Suppose the user-desired polarization direction $\vec{p}_d = \vec{e}_y$. According to (6) and (7), it can be known that on XOZ plane, the direction of $\vec{p}_{co}$ and $\vec{p}_X$ coincide with $\vec{e}_\phi$ and $\vec{e}_\theta$, respectively. We choose the same cosecant-squared function as that used in [21] for the desired mainlobe shape, and set $\Gamma_{SLL} = \Gamma_{XPL} = -22$ dB for the desired SLL and XPL. In the PSO algorithm, we set $N_p = 110$ for the population size and $M = 2000$ for the maximum number of iterations, and choose $W_1 = 5$ and $W_2 = W_3 = 1$ for the weighting factors in the fitness function. At the initial step ($k=0$), the proposed method also adopts analytical element patterns of rotated elements to find initial values of element rotations and phases, and the obtained CoP and XP patterns are also shown in Fig. 3(a). As can be seen, the obtained SLL of the synthesized CoP pattern is much lower than that of [21].

However, the pattern performance can change considerably if mutual coupling is included in practice. To illustrate this, a real rotated dipole array structure working at 3 GHz is built in which each dipole having length of 48 mm and diameter of 1 mm is rotated and excited according to the synthesized result in the initial step. The real array pattern is obtained by full-wave simulation using High Frequency Structure Simulator (HFSS) software [36], and it is also shown in Fig. 3(a) for comparison. It is observed that the real array pattern including mutual coupling deteriorates significantly in both sidelobe and mainlobe regions. The SLL increases from $-21.90$ dB to $-14.73$ dB.

To reduce the discrepancy between the synthesized pattern and the real array pattern (obtained by HFSS full-wave simulation), the proposed method adopts several refining steps to re-optimize the element rotations and phases, as described in Algorithm 1. By setting the scale factor $s = 1/3$, the angle range allowed for the element rotation becomes smaller and smaller as the number of refining steps increases. For example, the rotation angle range is $\pm\pi/6$, $\pm\pi/18$, and $\pm\pi/54$ for the 1th, 2nd and 3rd refining step. Fig. 3(b)-(d) show the synthesized and real array patterns using the rotations and phases obtained at three refining steps, respectively. As can be seen, as the number of refining steps increases, the synthesized pattern becomes more and more approaching to the real one. At the 3rd step, they become almost the same. At the 3rd step, the obtained SLL for the real array pattern is reduced to $-20.05$ dB, and the XPL is $-20.04$ dB. Compared with the result without the three refining steps, 5.32 dB reduction of the SLL is achieved. Fig. 4(a) shows the element rotations obtained at the initial step and the three refining steps, and Fig. 4(b) shows the excitation phases at these steps. Clearly, the synthesized rotations and phases are varied significantly from the initial step to the 1th refining step, while they change very little from the 2nd to 3rd refining step as expected. Performing a further refining step is unnecessary.

To study the effect of using different values of $s$ on the obtained pattern performance, we also test other cases of $s = 1/4$ and $s = 1/2$ for the proposed method. Table I lists the obtained SLL and XPL of the synthesized and real patterns by the proposed method with $s = [1/4, 1/3, 1/2]$ at different refining steps. From Table I, we can see that the proposed method with $s = 1/4$ obtains the highest final SLL ($-19.43$ dB) and XPL ($-19.95$ dB). This is mainly because that the available rotation range with $s = 1/4$ is not large enough. When the parameter $s$ increases, the obtained final pattern performance becomes better, as shown in the cases of $s = 1/3$ and $s = 1/2$. Compared with the case of $s = 1/3$, using $s = 1/2$ can obtain slightly better pattern performance in term of lower final SLL and XPL, but it requires four refining steps which costs more computational time. In the following examples, we still choose $s = 1/3$. With this choice, the proposed method usually requires only three refining steps while giving acceptable pattern performance. In this example, the obtained element rotation angles and phases with $s = 1/3$ are listed in the left column of Table II.

In this example, on the average the proposed method takes about 3.4 minutes for one time PSO-based optimization of 29 element rotations and phases in each iteration, and it takes about 53 minutes for one time HFSS full-wave simulation of the obtained 29-element rotated dipole array. Thus, the total time cost of the proposed method is about 3.8 hours. The test is performed on an Dell Workstation with an Intel Xeon E5-2697 CPU @2.30 GHz and 64 GB RAM.

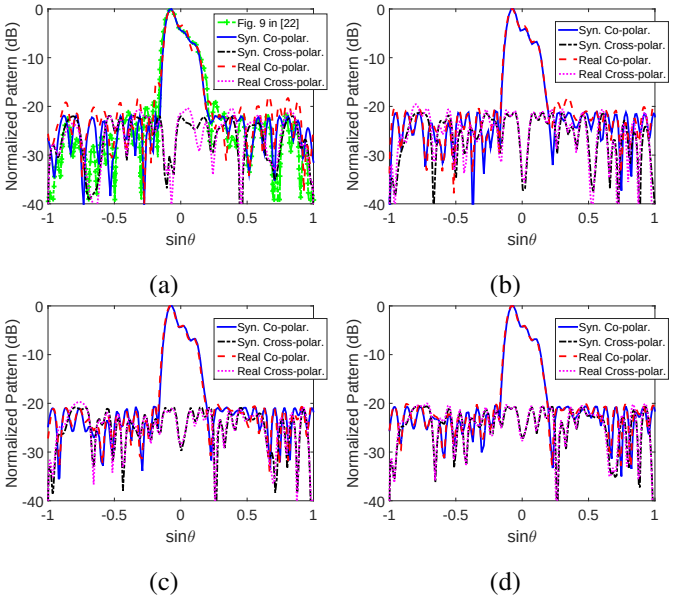


Fig. 3. The synthesized cosecant-squared CoP patterns and XP patterns by the proposed method at the initial step and three refining steps and the corresponding real array patterns obtained by full-wave simulation for the rotated dipole array. (a) shows the results at the initial step as well as the pattern shown in Fig. 9 of [22] for comparison, and (b)-(d) show the results at the 1th, 2nd and 3rd refining step, respectively.

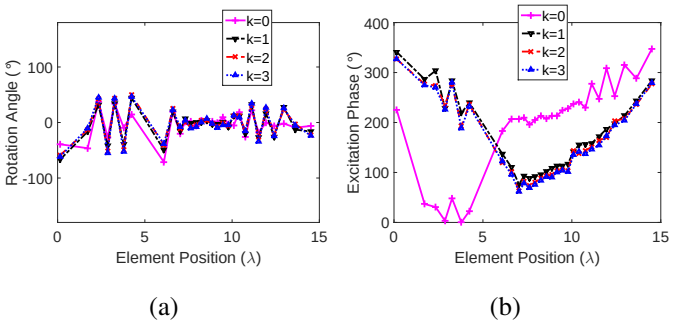


Fig. 4. The synthesized rotation angles and excitation phases by the proposed method at the initial and three refining steps for the cosecant-squared pattern case. (a) the rotation angles, and (b) the excitation phases.

### *B. Flat-top pattern synthesis for a rotated U-slot loaded microstrip antenna array*

In the second example, the proposed refined joint rotation/phase optimization method is utilized to synthesize a flat-top power pattern for a 24-element $0.55\lambda$-spaced linear array. To check the effectiveness of the proposed method for a more complicated antenna structure, we design a U-slot loaded microstrip antenna resonating at a center frequency of 10 GHz as the array element (analysis and design procedure for this

TABLE I THE MAXIMUM SLL AND XPL OF THE SYNTHESIZED AND REAL PATTERNS BY THE PROPOSED METHOD WITH DIFFERENT $s$ AT DIFFERENT REFINING STEPS FOR THE ROTATED DIPOLE ARRAY.

| $k$th | $s=1/4$ | | | | $s=1/3$ | | | | $s=1/2$ | | | |
|---|---|---|---|---|---|---|---|---|---|---|---|---|
| | Syn. Results (dB) | | Sim. Results (dB) | | Syn. Results (dB) | | Sim. Results (dB) | | Syn. Results (dB) | | Sim. Results (dB) | |
| | SLL | XPL | SLL | XPL | SLL | XPL | SLL | XPL | SLL | XPL | SLL | XPL |
| 0 | −21.90 | −21.93 | −14.73 | −20.32 | −21.90 | −21.93 | −14.73 | −20.32 | −21.90 | −21.93 | −14.73 | −20.32 |
| 1 | −20.62 | −20.71 | −19.39 | −18.79 | −20.91 | −21.23 | −18.07 | −19.56 | −21.34 | −21.41 | −18.31 | −18.98 |
| 2 | −19.73 | −19.91 | −19.70 | −19.85 | −20.65 | −20.82 | −20.04 | −19.71 | −21.01 | −21.23 | −19.13 | −20.53 |
| 3 | −19.61 | −19.90 | −19.43 | −19.95 | −20.42 | −20.62 | −20.05 | −20.04 | −20.72 | −20.88 | −20.26 | −19.24 |
| 4 | | | | | | | | | −20.68 | −20.75 | −20.41 | −20.48 |

TABLE II THE OBTAINED FINAL ROTATION ANGLES AND EXCITATION PHASES FOR THE COSECANT-SQUARED PATTERN IN EXAMPLE 1 AND THE FLAT-TOP PATTERN IN EXAMPLE 2.

| $n$ | Cosecant-Squared Pattern | | Flat-top Pattern | |
|---|---|---|---|---|
| | Rot. Angle (°) | Exc. Phase (°) | Rot. Angle (°) | Exc. Phase (°) |
| 1 | −61.31 | 327.00 | 119.73 | 165.34 |
| 2 | −10.31 | 274.54 | −61.96 | 306.40 |
| 3 | 45.11 | 270.27 | 44.40 | 282.69 |
| 4 | −55.01 | 226.00 | −32.43 | 250.32 |
| 5 | 43.21 | 280.70 | 22.65 | 221.29 |
| 6 | −52.33 | 188.97 | −13.69 | 200.44 |
| 7 | 46.60 | 232.17 | 10.22 | 188.27 |
| 8 | −38.41 | 122.29 | −2.90 | 184.39 |
| 9 | 22.33 | 96.27 | 4.45 | 158.99 |
| 10 | −7.92 | 62.31 | 0.10 | 136.94 |
| 11 | 3.54 | 78.03 | 1.71 | 106.78 |
| 12 | −10.33 | 68.91 | −0.25 | 98.89 |
| 13 | −7.80 | 75.85 | −0.31 | 96.88 |
| 14 | 0.79 | 83.53 | −0.23 | 99.48 |
| 15 | 6.90 | 91.60 | −0.98 | 111.80 |
| 16 | −1.82 | 90.68 | −1.91 | 142.52 |
| 17 | −9.65 | 100.83 | 0.23 | 160.35 |
| 18 | −4.14 | 104.54 | −2.17 | 178.29 |
| 19 | −4.30 | 101.48 | 0.26 | 193.03 |
| 20 | 12.75 | 135.02 | 2.79 | 207.40 |
| 21 | 9.59 | 141.98 | −2.10 | 214.73 |
| 22 | −15.36 | 137.50 | 0.11 | 281.43 |
| 23 | 34.12 | 146.54 | 4.91 | 233.75 |
| 24 | −34.50 | 154.65 | −179.58 | 158.09 |
| 25 | 27.10 | 172.70 | | |
| 26 | −24.39 | 194.80 | | |
| 27 | 25.86 | 203.89 | | |
| 28 | −5.06 | 237.17 | | |
| 29 | −23.40 | 279.05 | | |

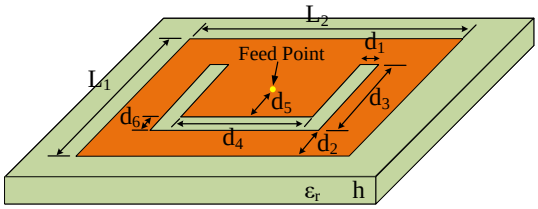


Fig. 5. Geometry of the U-slot loaded microstrip antenna element utilized in the flat-top pattern synthesis example. The parameters are given as follows: $d_1 = d_6 = 0.55$ mm, $d_2 = 1.85$ mm, $d_3 = 6.60$ mm, $d_4 = 4.40$ mm, $d_5 = 2.30$ mm, $h = 1.575$ mm, $L_1 = 9.40$ mm, $L_2 = 9.20$ mm, and $\varepsilon_r = 2.2$.

kind of antenna can be found in [37]). The geometry of the antenna model with detailed parameters are shown in Fig. 5. Assume the user-desired polarization direction is $\vec{p}_d = \vec{e}_y$. Then for the flat-top shaped pattern synthesis in XOZ plane, the CoP and XP are $\vec{e}_\phi$ and $\vec{e}_\theta$, respectively. The flat-top mainlobe region is chosen as $|\theta| \leq 9°$ while the sidelobe region is set as $|\theta| \geq 13°$. Set $\Gamma_{SLL} = \Gamma_{XPL} = -16$ dB and $N_p = 60$ in this example, and other parameters including $M$, $W_1$, $W_2$ and $W_3$ are the same as those in

TABLE III THE MAXIMUM SLL, XPL AND MAINLOBE RIPPLE OF THE SYNTHESIZED AND REAL ARRAY PATTERNS AT THE INITIAL AND THREE REFINING STEPS FOR THE ROTATED U-SLOT MICROSTRIP ANTENNA ARRAY.

| $k$th | Synthesized Results (dB) | | | Simulated Results (dB) | | |
|---|---|---|---|---|---|---|
| | SLL | XPL | Ripple | SLL | XPL | Ripple |
| 0 | −15.85 | −15.97 | ±0.45 | −12.75 | −13.11 | ±0.73 |
| 1 | −15.23 | −15.57 | ±0.55 | −13.92 | −15.23 | ±0.44 |
| 2 | −15.09 | −15.14 | ±0.44 | −13.98 | −13.92 | ±0.45 |
| 3 | −14.94 | −14.74 | ±0.65 | −14.58 | −14.57 | ±0.58 |

the first example. At the initial step, the vectorial element pattern is obtained by simulating the U-slot loaded microstrip antenna with periodic boundaries, and the flat-top pattern is then synthesized by finding appropriate rotation angles and excitation phases without considering the variation of mutual coupling. Clearly, the synthesized array pattern would be different from the real one obtained by full-wave simulation of the rotated array, as shown in Fig. 6(a). The synthesized SLL, XPL and mainlobe ripple are −15.85 dB, −15.97 dB and ±0.45 dB, respectively, while for the real pattern, they increase to −12.75 dB, −13.11 dB and ±0.73 dB, respectively. To improve the real pattern performance, three refining steps are conducted to successively refine the optimized rotations and phases. Fig. 6(b)-(d) show the synthesized and real array patterns at the three refining steps, respectively. As can be seen, the synthesized pattern matches the real pattern better and better as the number of refining steps increases. Table III lists all the maximum SLL, XPL and mainlobe ripple for both synthesized and real array patterns at different refining steps. At the 3rd step, the obtained SLL and XPL for the real pattern are −14.58 dB and −14.57 dB, which are very close to the corresponding synthesized ones. Fig. 7(a) shows the element rotations obtained at the initial step and three refining steps, and Fig. 7(b) shows the excitation phases at these steps. The obtained final element rotations and phases after three refining steps can be found in the right column of Table II. As can be seen, some edge elements of the obtained array have much different rotation angles. These rotation angles would be very hard to find without a systematic approach. In this example, it takes about 2.2 minutes for one time PSO-based optimization of 24 rotations and phases, and 3 hours for one time HFSS full-wave simulation of the obtained 24-element rotated U-slot loaded patch antenna array on the same computer as the first example. Hence, the total time cost is about 12.1 hours for this example.

In addition, we also apply phase-only optimization by using PSO algorithm to synthesize the same desired pattern. In this

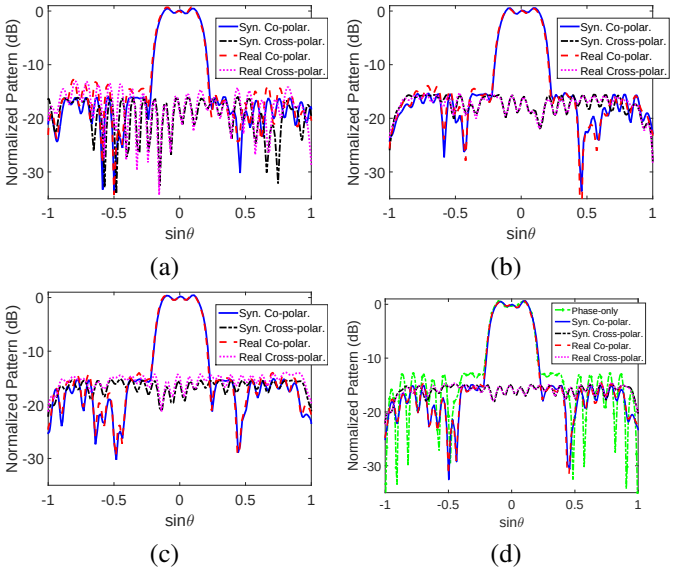


Fig. 6. The synthesized flat-top CoP patterns and XP patterns by the proposed method at the initial step and three refining steps and the corresponding real array patterns obtained by full-wave simulation for the rotated U-slot loaded microstrip antenna array. (a) shows the results at the initial step, and (b)-(d) show the results at the 1th, 2nd and 3rd refining step, respectively. The synthesized pattern by the phase-only optimization is also shown in (d).

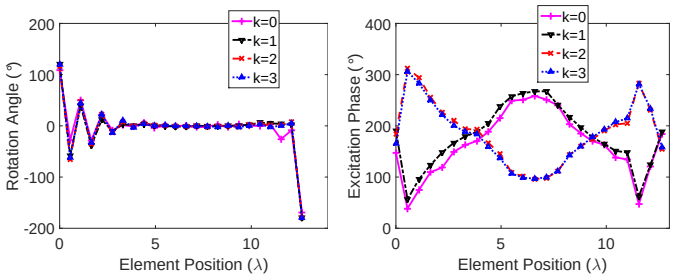


Fig. 7. The synthesized rotation angles and excitation phases by the proposed method at the initial and three refining steps for the flat-top pattern case. (a) the rotation angles, and (b) the excitation phases.

test, a linear array with 24 non-rotated U-slot loaded microstrip antenna elements (the element is the same as that of the rotated array) is built, and the active element patterns are obtained by using full-wave simulation. The obtained pattern by phase-only optimization is shown in Fig. 6(d) as well. As can be seen, compared with the final pattern obtained by the proposed method, the synthesized pattern by the phase-only optimization has almost the same mainlobe shape but with a much higher SLL of $-12.77$ dB. This further validates the advantage of the proposed method.

### *C. Circular flat-top pattern synthesis for a planar array with rotated cavity-backed patch antennas*

In the last example, we check the effectiveness of the proposed refined joint rotation/phase optimization method for synthesizing a shaped power pattern for a planar array. In [9], a circular flat-top pattern was synthesized by optimizing both amplitudes and phases of a $11 \times 11$ $\lambda/2$-spaced array without considering mutual coupling. This pattern has a circular flat-top mainlobe in the region of $\{\theta \leq 15^\circ$ and $\phi \in (0^\circ, 360^\circ)\}$ and the maximum SLL is less than $-10$ dB in the region of $\{\theta \geq 20^\circ$ and $\phi \in (0^\circ, 360^\circ)\}$, as shown in Fig. 4 (a) of [9]. For the proposed method, the same size of a planar array is used and a cavity-backed patch antenna presented in [38] is adopted as the array element. Suppose the user-desired polarization direction is still $\vec{p}_d = \vec{e}_y$. Unlike the linear array pattern synthesis cases, $\vec{e}_\phi$ and $\vec{e}_\theta$ are no longer CoP and XP directions in the planar array case. The realizable CoP and XP directions will always change with the propagation direction $(\theta, \varphi)$ according to (6) and (7). In this example, we take the same circular flat-top function as the desired mainlobe shape. Set $\Gamma_{SLL} = \Gamma_{XPL} = -11$ dB and $N_p = 400$. Other parameters including $M$, $W_1$, $W_2$ and $W_3$ are still used as the same as those in the first example. Table IV lists the obtained maximum SLL, XPL and mainlobe ripple for both synthesized and real array patterns at the initial and three refining steps. The obtained SLL and XPL for the real pattern decrease as the refining procedure is performed. At the 3rd refining step, the obtained real SLL, XPL and the mainlobe ripple are $-10.32$ dB, $-10.18$ dB and $\pm 1.23$ dB, respectively. Fig. 8(a)-(d) show the top views of CoP and XP components of the synthesized and real array patterns (obtained by using full-wave simulation) at the 3rd step. As can be seen, the final synthesized and real patterns agree well with each other in both CoP and XP components. For more clear observation, the $\phi$-cut patterns of real CoP and XP patterns are depicted in Fig. 8(e) and (f). Compared with the result in Fig. 4(a) of [9], the current obtained pattern including mutual coupling has better sidelobe performance. Fig. 9 shows the obtained array arrangement with optimized element rotations. This array does not apply amplitude weighting so that many of unequal power dividers are not required any more. In this example, it takes about 4.1 hours for one time PSO-based optimization, and 7.8 hours for one time HFSS full-wave simulation of the obtained 121-element cavity-backed antenna planar array. The total time cost is about 47.6 hours for this example.

TABLE IV THE MAXIMUM SLL, XPL AND MAINLOBE RIPPLE OF THE SYNTHESIZED AND REAL ARRAY PATTERNS AT THE INITIAL AND THREE REFINING STEPS FOR THE PLANAR ARRAY WITH ROTATED CAVITY-BACKED PATCH ANTENNAS.

| $k$th | Synthesized Results (dB) | | | Simulated Results (dB) | | |
|---|---|---|---|---|---|---|
| | SLL | XPL | Ripple | SLL | XPL | Ripple |
| 0 | $-10.62$ | $-10.83$ | $\pm 1.14$ | $-7.57$ | $-8.25$ | $\pm 1.60$ |
| 1 | $-10.77$ | $-10.63$ | $\pm 1.09$ | $-9.25$ | $-9.88$ | $\pm 1.19$ |
| 2 | $-10.30$ | $-10.20$ | $\pm 1.14$ | $-9.83$ | $-10.39$ | $\pm 1.17$ |
| 3 | $-10.32$ | $-10.32$ | $\pm 1.17$ | $-10.32$ | $-10.18$ | $\pm 1.23$ |

## IV. MEASUREMENT RESULTS

A prototype of the 24-element rotated U-slot antenna array in example 2 is fabricated on a three-layered substrate as shown in Fig. 10. The experimental array consists of the rotated U-slot antennas, the RF ground and the feeding network. The feeding network is designed as a multi-stage equal power dividers followed by phase-shifter lines which provides the required excitation phases. 24 metal via holes which insulated from the RF ground are made to connect the feeding lines

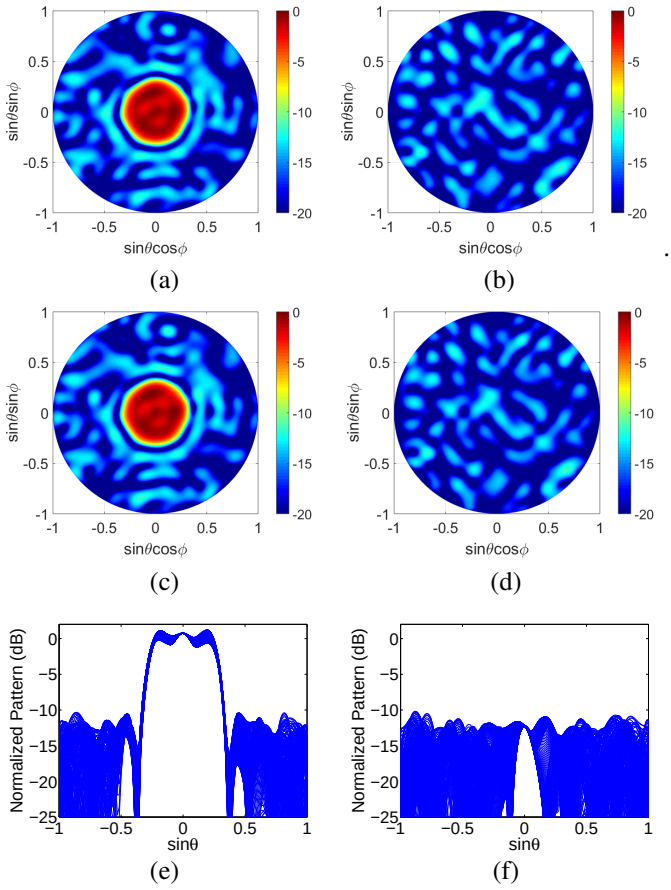


Fig. 8. The synthesized circular flat-top CoP and XP patterns by the proposed method and the corresponding real array patterns obtained by full-wave simulation. (a) and (b) show the synthesized CoP and XP patterns; (c) and (d) show the real CoP and XP patterns; (e) and (f) show different $\phi$-cuts of the real CoP and XP patterns.

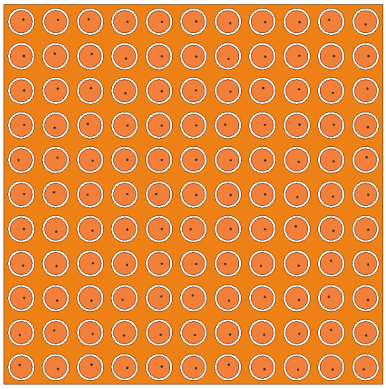

Fig. 9. The obtained element-rotated planar array by the proposed method in the circular flat-top pattern synthesis example.

and the antennas. The upper and lower layers of dielectric have the same relative permittivity $\varepsilon_r = 2.2$ but with different dimensions. The dimension of the upper layer dielectric is $429$ mm $\times$ $131$ mm with thickness of $1.575$ mm, and dimension of the lower layer dielectric is $429$ mm $\times$ $58$ mm with thickness of $0.508$ mm. Since the dielectric layer is so thin and long, a hard plastic plate is stuck together with the lower dielectric to keep the whole structure flat.

This antenna array prototype is measured using a far-field

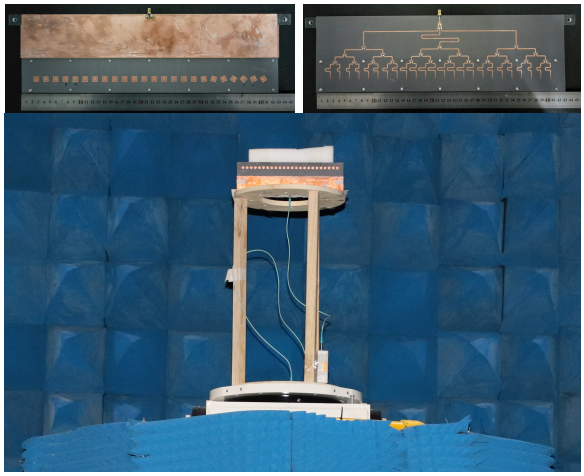

Fig. 10. The fabricated 24-element rotated U-slot microstrip antenna array with a feeding network and a supportive plastic plate, as well as the photo of this array under the test.

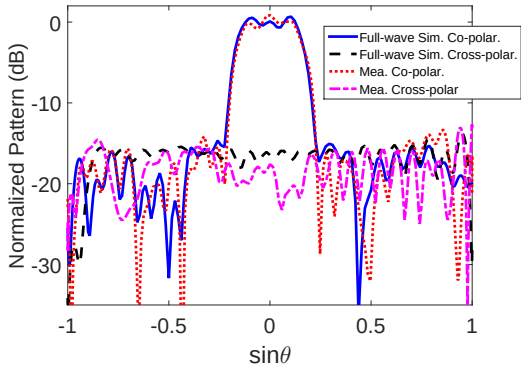


Fig. 11. The measured CoP and XP patterns as well as the full-wave simulation results for the 24-element rotated U-slot antenna array integrated with the feeding network.

measurement system in a microwave anechoic chamber located at Haiyun Campus, Xiamen University. The measured CoP and XP patterns along with the HFSS simulated patterns are drawn together in Fig. 11. Note that different from the simulated patterns in Fig. 6(d) (fed by 24 individual coaxial ports in HFSS model), the real patterns depicted in Fig. 11 is obtained by simulating the element-rotated array fed by the designed feeding network. Hence, there is a little bit deviation between the real patterns in Fig. 6(d) and that in Fig. 11. As can be seen in Fig. 11, the mainlobe ripple of the measured CoP pattern is $\pm 0.84$ dB which is slightly higher than the simulated ripple of $\pm 0.67$ dB. The measured SLL and XPL are $-13.33$ dB and $-12.67$ dB, respectively, which are $1.27$ dB and $1.11$ dB higher than those of the simulated patterns, respectively. Although there exists a small performance degradation probably due to some fabrication errors and non-ideal measurement environment, the measured CoP and XP patterns in general agree well with the full-wave simulation results.

## V. Conclusion

A refined joint element rotation/phase optimization strategy has been presented to synthesize vectorial shaped power

patterns for linear and planar antenna arrays with arbitrary element structures including mutual coupling. This strategy is a significant extension of the original joint rotation/phase optimization technique used only for synthesizing linear array with ideally rotated dipoles where an analytical dipole pattern expression is used and mutual coupling effect for practical antenna arrays cannot be considered. For a more general antenna array, the key problem of synthesizing vectorial shaped power pattern by using joint element rotation/phase optimization is that we do not know the pattern expression for an element-rotated array with rotation angles to be optimized. The proposed refined optimization strategy provides a very useful solution. Three synthesis examples have been provided, including synthesizing a 29-element rotated coupled dipole array with cosecant-squared pattern, a 24-element rotated U-slot loaded microstrip antenna array with flat-top pattern, a planar rotated cavity-backed patch antenna array with circular flap-top pattern. Synthesis results show that the refined rotation/phase optimization strategy is indeed effective and robust for obtaining vectorial shaped patterns for different antenna arrays. The synthesized array patterns can produce the desired CoP mainlobe shapes while maintaining reasonable SLL and XPL control. Measured results from an experimental 24-element rotated U-slot microstrip antenna array agree well with the simulated results.

Finally, it is noted the proposed strategy does not require the nonuniform amplitude weighting used in conventional shaped pattern synthesis methods, thus avoiding the use of many unequal power dividers. It provides a novel shaped pattern synthesis technique for linear and planar arrays.

## REFERENCES


[1] P. M. Woodward and J. D. Lawson, "The theoretical precision with which an arbitrary radiation pattern may be obtained from a source of a finite size," *J. IEE*, vol. 95, no. 37, pt. III, pp. 363-370, Sep. 1948.

[2] J.-Y. Li, Y.-X. Qi, and S.-G. Zhou, "Shaped beam synthesis based on superposition principle and Taylor method," *IEEE Trans. Antennas Propag.*, vol. 65, no. 11, pp. 6157-6160, Sep. 2017.

[3] J. L. A. Quijano and G. Vecchi, "Alternating adaptive projections in antenna synthesis," *IEEE Trans. Antennas Propag.*, vol. 58, no. 3, pp. 727-737, Mar. 2010.

[4] A. Haddadi, A. Ghorbani, and J. Rashed-Mohassel, "Cosecant-squared pattern synthesis using a weighted alternating reverse projection method," *IET Microw., Antennas Propag.*, vol. 5, Iss. 15, pp. 1789-1795, 2011.

[5] K. Yang, Z. Zhao, and Q. H. Liu, "An iterative FFT based flat-top footprint pattern synthesis method with planar array," *J. Electromagn. Waves Appl.*, vol. 26, pp. 1956-1966, Oct. 2012.

[6] W.-T. Li, Y.-Q. Hei, J. Yang, and X.-W. Shi, "Synthesis of multiple-pattern planar arrays with a hybrid generalised iterative fast Fourier transform algorithm," *IET Microw., Antennas Propag.*, vol. 10, Iss. 1, pp. 16-24, Jan. 2016.

[7] Y. Liu, X. Huang, K. D. Xu, Z. Song, S. Yang, and Q. H. Liu, " Pattern synthesis of unequally spaced linear arrays including mutual coupling using iterative FFT via virtual active element pattern expansion," *IEEE Trans. Antennas Propag.*, vol. 65, no. 8, pp. 3950-3958, Aug. 2017.

[8] K. M. Tsui and S. C. Chan, "Pattern synthesis of narrowband conformal arrays using iterative second-order cone programming," *IEEE Trans. Antennas Propag.*, vol. 58, no. 6, pp. 1959-1970, Jun. 2010.

[9] B. Fuchs, A. Skrivervik, and J. R. Mosig, "Shaped beam synthesis of arrays via sequential convex optimizations," *IEEE Antennas Wireless Propag. Lett.*, vol. 12, pp. 1049-1052, Aug. 2013.

[10] J. I. Echeveste, M. A. G. de Aza, and J. Zapata, "Shaped beam synthesis of real antenna arrays via finite-element method, floquet modal analysis, and convex programming," *IEEE Trans. Antennas Propag.*, vol. 64, no. 4, pp. 1279-1286, Apr. 2016.

[11] B. Fuchs, "Application of convex relaxation to array synthesis problems," *IEEE Trans. Antennas Propag.*, vol. 62, no. 2, pp. 634-640, Feb. 2014.

[12] Y. Liu, J. Bai, K. D. Xu, Z. Xu, F. Han, Q. H. Liu, and Y. Jay Guo, "Linearly polarized shaped power pattern synthesis with sidelobe and cross-polarization control by using semidefinite relaxation," *IEEE Trans. Antennas Propag.*, vol. 66, no. 6, pp. 3207-3212, Jun. 2018.

[13] F. J. Ares-Pena, J. A. Gonzalez, E. Lopez, and S. R. Rengarajan, "Genetic algorithms in the design and optimization of antenna array patterns," *IEEE Trans. Antennas Propag.*, vol. 47, no. 3, pp. 506-510, Mar. 1999.

[14] P. You, Y. Liu, K. D. Xu, C. Zhu, and Q. H. Liu, "Generalisation of genetic algorithm and fast Fourier transform for synthesising unequally spaced linear array shaped pattern including coupling effects," *IET Microw., Antennas Propag.*, vol. 11, no. 6, pp. 827-832, May 2017.

[15] A. A. Akdagli, K. Guney, and D. Karaboga, "Touring ant colony optimization algorithm for shaped-beam pattern synthesis of linear antenna," *Electromagnetics*, vol. 26, pp. 615-628, 2006.

[16] A. Pirhadi, M. H. Rahmani, and A. Mallahzadeh, "Shaped beam array synthesis using particle swarm optimisation method with mutual coupling compensation and wideband feeding network," *IET Microw., Antennas Propag.*, vol. 8, no. 8, pp. 549-555, Jun. 2014.

[17] A. Trastoy, F. Ares, and E. Moreno, "Phase-only control of antenna sum and shaped patterns through null perturbation," *IEEE Antennas Propag. Mag.*, vol. 43, no. 6, pp. 45-54, Dec. 2001.

[18] L. Marcaccioli, R. V. Gatti, and R. Sorrentino, "Series expansion method for phase-only shaped beam synthesis and adaptive nulling," in *Proc. URSI Int. Symp. Electromagn. Theory (EMTS)*, Pisa, Italy, 2004, pp. 676-678.

[19] D. P. Scholnik, "A parameterized pattern-error objective for large-scale phase-only array pattern design," *IEEE Trans. Antennas Propag.*, vol. 64, no. 1, pp. 89-98, Jan. 2016

[20] J. Liang, X. Fan, W. Fan, D. Zhou, and J. Li, "Phase-only pattern synthesis for linear antenna arrays," *IEEE Antennas Wireless Propag. Lett.*, vol. 16, pp. 3232-3235, Nov. 2017.

[21] O. M. Bucci, T. Isernia, and A. F. Morabito, "An effective deterministic procedure for the synthesis of shaped beams by means of uniform-amplitude linear sparse arrays," *IEEE Trans. Antennas Propag.*, vol. 61, no. 1, pp. 169-175, Jan. 2013

[22] R. L. Haupt and D. W. Aten, "Low sidelobe arrays via dipole rotation," *IEEE Trans. Antennas Propag.*, vol. 57, no. 5, pp. 1575-1579, May 2009.

[23] M. Li, Y. Liu, S.-L. Chen, P.-Y. Qin, and Y. J. Guo, "Low sidelobe synthesis of dipole arrays by element orientation selection using binary codec genetic algorithm," in *Proc. 11th Eur. Conf. Antennas Propag.*, Paris, France, Mar. 2017, pp. 2838-2840.

[24] A. B. Smolders and H. J. Visser, "Low side-lobe circularly-polarized phased arrays using a random sequential rotation technique," *IEEE Trans. Antennas Propag.*, vol. 62, no. 12, pp. 6476-6481, Sep. 2014.

[25] A. B. Smolders, S. J. Geluk, and A. C. F. Reniers, "Circularly-polarized sparse arrays realized by randomly-rotated linearly-polarized antennas," *IEEE Antennas Wireless Propag. Lett.*, vol. 16, pp. 736-739, Aug. 2016.

[26] J. I. Echeveste, J. Rubio, M. Á. G. de Aza, and C. Craeye, "Pattern synthesis of coupled antenna arrays via element rotation," *IEEE Antennas Wireless Propag. Lett.*, vol. 16, pp. 1707-1710, Feb. 2017.

[27] M. Li, Y. Liu, and Y. J. Guo, "Shaped power pattern synthesis of a linear dipole array by element rotation and phase optimization using dynamic differential evolution," *IEEE Antennas Wireless Propag. Lett.*, vol. 17, no. 4, pp. 697-701, Mar. 2018.

[28] D. F. Kelley and W. L. Stutzman, "Array antenna pattern modeling methods that include mutual coupling effects," *IEEE Trans. Antennas Propag.*, vol. 41, no. 12, pp. 1625-1632, Dec. 1993.

[29] J. Ouyang, X. Luo, J. Yang, K. Z. Zhang, J. Zhang, and F. Yang, "Analysis and synthesis of conformal conical surface linear phased array with volume surface integral equation+AEP (active element pattern) and INSGA-II," *IET Microw., Antennas Propag.*, vol. 6, no. 11, pp. 1277-1285, Aug. 2012.

[30] A. Ludwig, "The definition of cross polarization," *IEEE Trans. Antennas Propag.*, vol. 21, no. 1, pp. 116-119, 1973.

[31] R. C. Eberhart and Y. Shi, "Particle swarm optimization: developments, applications and resources," in *Proc. IEEE Congr. Evol. Comput.*, Seoul, Korea, 2001, pp. 81-86.

[32] J. Kennedy and R. Eberhart, "Particle swarm optimization," in *Proc. IEEE Int. Conf. Neural Networks*, Perth, Australia, 1995, vol. 4, pp. 1942-1948.

[33] J. Robinson and Y. Rahmat-Samii, "Particle swarm optimization in electromagnetics, *IEEE Trans. Antennas Propag.*, vol. 52, no. 2, pp. 397-407, Feb. 2004.

[34] L. Poli, P. Rocca, L. Manica, and Andrea Massa, "Handling sideband radiations in time-modulated arrays through particle swarm optimization," *IEEE Trans. Antennas Propag.*, vol. 58, no. 4, pp. 1408-1411, Apr. 2010.
[35] S.-H. Yang and J.-F. Kiang, "Adjustment of beamwidth and side-lobe level of large phased-arrays using particle swarm optimization technique," *IEEE Trans. Antennas Propag.*, vol. 62, no. 1, pp. 138-144, Jan. 2014.
[36] Ansoft High Frequency Structure Simulator (HFSS), Ver. 15, Ansoft Corp., Pittsburgh, PA, USA, 2013.
[37] S. Weigand, G. H. Huff, K. H. Pan, and J. T. Bernhard, "Analysis and design of broad-band single-layer rectangular U-slot microstrip patch antennas," *IEEE Trans. Antennas Propag.*, vol. 51, no. 3, pp. 457-468, May 2003.
[38] J. I. Echeveste, M. A. G. de Aza , J. Rubio, and J. Zapata. "Near-optimal shaped-beam synthesis of real and coupled antenna arrays via 3-D-FEM and phase retrieval," *IEEE Trans. Antennas Propag.*, vol. 64, no. 6, pp. 2189-2196, Mar. 2016.

**Yanhui Liu** (M'2015-SM'2019) received the B.S. and Ph.D. degrees both in electrical engineering from the University of Electronic Science and Technology of China (UESTC) in 2004 and 2009, respectively.

From September 2007 to June 2009, he was a Visiting Scholar in the Department of Electrical Engineering at Duke University, Durham, NC. In July 2011, he joined in the Department of Electronic Science, Xiamen University, China, where he was lately promoted as a Full Professor. From September to December in 2017, he was a Visiting Professor at State Key Laboratory of Millimeter Waves in City University of Hong Kong. From December 2017, he has been with Global Big Data Technologies Centre, University of Technology Sydney (UTS) as a Visiting Professor/Research Principal. From January 2020, he is a Professor at UESTC where he is supported by "100 Talents Plan of UESTC". He received the UESTC Outstanding Graduate Award in 2004, and the Excellent Doctoral Dissertation Award of Sichuan Province of China in 2011. He has authored and co-authored over 140 peer-reviewed journal and conference papers including 80 SCI-indexed papers. He holds 17 Chinese invention patents in antennas and applied electromagnetics.

Dr. Liu is serving as a reviewer for a dozen of SCI-indexed journals. Since 2018, he has served as an Associate Editor for the IEEE Access. He has served many times as TPC member or reviewer in IEEE APS, PIERS, APCAP, ACES and NCANT, and served as a session chair in NCANT2015, PIERS2016/2019, ACES2017-China, NCANT2017, APCAP2017, and ICCEM2018/2019. His research interests include antenna array design, reconfigurable antennas, and electromagnetic scattering and imaging.

**Ming Li** was born in Anhui, China, in 1991. He received the B.S. degree in electronic information science and technology and M.S. degree in electromagnetic field and microwave technology from Xiamen University, Xiamen, China, in 2015 and 2018, respectively. He is currently pursuing the Ph.D. degree with the Global Big Data Technologies Centre (GBDTC) of the University of Technology Sydney (UTS), Australia. His current research interests include the antenna array design and reconfigurable antennas.

**Randy L. Haupt** (M'82-SM'90-F'00) received the B.S. degree in electrical engineering from the U.S. Air Force Academy, CO, USA, the M.S. degree in engineering management from Western New England College, Springfield, MA, USA, in 1981, the M.S. degree in electrical engineering from Northeastern University, Boston, MA, USA, in 1983, and the Ph.D. degree in electrical engineering from the University of Michigan, Ann Arbor, MI, USA, in 1987. Currently, he is a Professor of Electrical Engineering, Colorado School of Mines, Golden, CO, USA. Previously, he was an RF Staff Consultant with Ball Aerospace & Technologies Corp., Senior Scientist, and Department Head with the Applied Research Laboratory of Pennsylvania State University, Professor and Department Head of ECE with Utah State, Professor and Chair of EE with the University of Nevada Reno, and Professor of EE with the USAF Academy. He was a Project Engineer for OTH-B radar and a Research Antenna Engineer for Rome Air Development Center early in his career. He retired as a lieutenant colonel from the U.S. Air Force in 1997. He is the coauthor of the books Practical Genetic Algorithms (2nd ed., Wiley, 2004), Genetic Algorithms in Electromagnetics (Wiley, 2007), and Introduction to Adaptive Antennas (SciTech, 2010), as well as the author of Wireless Communications Systems An Introduction (Wiley, 2020), Antenna Arrays a Computation Approach (Wiley, 2010), and Timed Arrays (Wiley, 2015). Dr. Haupt was the Federal Engineer of the Year in 1993. He serves as the Associate Editor for the"Ethically Speaking" columns in the AP-S Magazine and Radio Science Bulletin.

**Y. Jay Guo** (Fellow2014) received a Bachelor Degree and a Master Degree from Xidian University in 1982 and 1984, respectively, and a PhD Degree from Xian Jiaotong University in 1987, all in China. His research interest includes antennas, mm-wave and THz communications and sensing systems as well as big data technologies. He has published over 470 research papers including 250 journal papers, and holds 26 patents in antennas and wireless systems. He is a Fellow of the Australian Academy of Engineering and Technology, a Fellow of IEEE and a Fellow of IET, and was a member of the College of Experts of Australian Research Council (ARC, 2016-2018). He has won a number of most prestigious Australian Engineering Excellence Awards (2007, 2012) and CSIRO Chairmans Medal (2007, 2012), and was named one of the most influential engineers in Australia in 2014 and 2015, respectively.

Prof Guo is a Distinguished Professor and the Director of Global Big Data Technologies Centre (GBDTC) at the University of Technology Sydney (UTS), Australia. Prior to this appointment in 2014, he served as a Director in CSIRO for over nine years. Before joining CSIRO, he held various senior technology leadership positions in Fujitsu, Siemens and NEC in the U.K.

Prof Guo has chaired numerous international conferences and served as guest editors for a number of IEEE publications. He is the Chair of International Steering Committee, International Symposium on Antennas and Propagation (ISAP). He was the International Advisory Committee Chair of IEEE VTC2017, General Chair of ISAP2022, ISAP2015, iWAT2014 and WPMC'2014, and TPC Chair of 2010 IEEE WCNC, and 2012 and 2007 IEEE ISCIT. He served as Guest Editor of special issues on "*Antennas for Satellite Communications*" and "*Antennas and Propagation Aspects of 60-90GHz Wireless Communications*," both in IEEE Transactions on Antennas and Propagation, Special Issue on "*Communications Challenges and Dynamics for Unmanned Autonomous Vehicles*," IEEE Journal on Selected Areas in Communications (JSAC), and Special Issue on "*5G for Mission Critical Machine Communications*", IEEE Network Magazine.